A new approach for generating bispecific antibodies based on a common light chain format and the stable architecture of human immunoglobulin G_1

Received for publication, April 28, 2017, and in revised form, June 14, 2017 Published, Papers in Press, June 27, 2017, DOI 10.1074/jbc.M117.793497

Camilla De Nardis[‡1], Linda J. A. Hendriks[§1], Emilie Poirier[¶], Tudor Arvinte[¶‖], Piet Gros[‡], Alexander B. H. Bakker[§], and John de Kruif[§2]

From the [‡]Crystal and Structural Chemistry Group, Bijvoet Center for Biomolecular Research, Department of Chemistry, Faculty of Science, Utrecht University, 3584 CH Utrecht, The Netherlands, [§]Merus N.V., 3584 CM Utrecht, The Netherlands, [¶]Therapeomic Inc., CH-4002 Basel, Switzerland, and the [‖]University of Geneva, CH-1211 Geneva, Switzerland

Edited by Peter Cresswell

Bispecific antibodies combine two different antigen-binding sites in a single molecule, enabling more specific targeting, novel mechanisms of action, and higher clinical efficacies. Although they have the potential to outperform conventional monoclonal antibodies, many bispecific antibodies have issues regarding production, stability, and pharmacokinetic properties. Here, we describe a new approach for generating bispecific antibodies using a common light chain format and exploiting the stable architecture of human immunoglobulin G_1. We used iterative experimental validation and computational modeling to identify multiple Fc variant pairs that drive efficient heterodimerization of the antibody heavy chains. Accelerated stability studies enabled selection of one Fc variant pair dubbed "DEKK" consisting of substitutions L351D and L368E in one heavy chain combined with L351K and T366K in the other. Solving the crystal structure of the DEKK Fc region at a resolution of 2.3 Å enabled detailed analysis of the interactions inducing CH3 interface heterodimerization. Local shifts in the IgG backbone accommodate the introduction of lysine side chains that form stabilizing salt-bridge interactions with substituted and native residues in the opposite chain. Overall, the CH3 domain adapted to these shifts at the interface, yielding a stable Fc conformation very similar to that in wild-type IgG. Using the DEKK format, we generated the bispecific antibody MCLA-128, targeting human EGF receptors 2 and 3. MCLA-128 could be readily produced and purified at industrial scale with a standard mammalian cell culture platform and a routine purification protocol. Long-term accelerated stability assays confirmed that MCLA-128 is highly stable and has excellent biophysical characteristics.

Bispecific antibodies (bsAbs)[3] combine two different antigen-binding sites in a single molecule. Bispecific antibodies can address multiple antigens in a single molecule resulting in more specific targeting, novel mechanisms of action, and higher clinical efficacies (1). Numerous technical solutions are available for linking the two different antibody specificities (2). Extensive engineering of therapeutic proteins may, however, generate molecules whose drug-like properties, such as production yields, stability, and half-life, are less favorable. Bispecific molecules that remain faithful to the natural IgG format use a structure shaped by a million years of evolution. Drugs based on such molecules are therefore more likely to have pharmacokinetic properties similar to the natural antibody.

Conventional IgG antibodies are bivalent and monospecific, and their assembly depends upon the homodimerization of the so-called crystallizable fragment (Fc). The process is mediated by the association of two identical heavy chains (HCs) followed by the assembly of two identical light chains (LCs). The Fc portion of an IgG is composed of a hinge region, a CH2 domain, and a CH3 domain, with the CH3 domain forming the dimerization interface. In the production of bispecific IgG, heterodimer formation can thus be induced by engineering the CH3 domains such that homodimer-favoring interactions are replaced by asymmetric interactions. Most bispecific formats based on native IgG benefit from the use of a common light chain (cLC) (3, 4), which has the advantage of preventing mispairing of heavy and light chains without the need for engineering.

Different structure-based design strategies have so far been adopted for the production of heterodimeric CH3 variant pairs, and these have recently been reviewed by Ha *et al.* (4). Annealing-based approaches for producing bispecific antibodies by mixing two different antibody components are also being pursued (5). Other native formats are rat–mouse hybrids or IgG_1–IgG_3 hybrids (6), in which there is no preferential pairing between heavy chains. Purification of these bsAbs

This work was supported by BioStruct-X Grant 283570 embedded in the European Union's Seventh Framework Programme FP7/2007-2013. L. H., A. B., and J. d. K. are employees and shareholders of Merus N.V.
This article was selected as one of our Editors' Picks.
This article contains supplemental Tables S1–S2.
The atomic coordinates and structure factors (codes 5NSC and 5NSG) have been deposited in the Protein Data Bank (http://wwpdb.org/).

[1] Both authors contributed equally to this work.
[2] To whom correspondence should be addressed: Merus N.V., Yalelaan 62, 3584CM Utrecht, The Netherlands. Tel.: 31-30-2538804; E-mail: j.dekruif@merus.nl.

[3] The abbreviations used are: bsAb, bispecific antibody; Bistris, 2-[bis(2-hydroxyethyl)amino]-2-(hydroxymethyl)propane-1,3-diol; PDB, Protein Data Bank; HC, heavy chain; LC, light chain; cLC, common light chain; nMS, native mass spectrometry; r.m.s.d., root-mean-square deviation; CEX, cation-exchange chromatography; PEI, polyetheleneimine; 1,8-ANS, 1-anilinonaphthalene-8-sulfonic acid; DSC, differential scanning calorimetry.

relies on their differential binding affinity for purification matrices.

Challenges encountered during bispecific IgG generation using CH3 engineering include loss of stability relative to the natural Fc and the presence of homodimer contaminations. In this study, we therefore aimed to identify Fc variant pairs that enable efficient formation of IgG heterodimers while maintaining the stability of the natural Fc region. Taking a novel charge–introduction approach, we first identified residues within the CH3 interface that impaired the formation of IgG homodimers. Based on this information, variant pairs were designed and analyzed for their efficiency of heterodimer formation. The charge pair that had the most favorable heterodimer/homodimer ratio was used in a computational approach called HADDOCK (High Ambiguity Driven protein-protein Docking) (7, 8), an information-driven docking tool for modeling biomolecular complexes. This generated several candidates for further experimental analysis. The screening resulted in the selection of the Fc variant pair "DEKK," which contained the substitutions L351D,L368E in one heavy chain and L351K,T366K in the other. The crystal structure of the Fc region of DEKK was determined at a resolution of 2.3 Å, which revealed the molecular interactions at the dimerization interface.

Finally, the DEKK Fc variant pair was used to construct MCLA-128, a bispecific humanized full-length IgG_1 antibody. This bsAb specifically targets the human epidermal growth factor receptors (HER) 2 and 3 and is currently undergoing clinical phase I/II evaluation in patients with solid tumors (NCT02912949). MCLA-128 was produced and purified at industrial scale, and a liquid formulation was identified in which the protein was shown to have excellent long-term stability.

Results

Charged residues were introduced at different positions within the CH3 interface to identify those substitutions that interfere with IgG homodimer formation (Table 1). The constructs were expressed and analyzed using non-reducing SDS-PAGE. Constructs containing CH3 interfaces that allowed homodimer formation are visible as bands at 144 kDa, whereas interference with dimer formation is demonstrated by the presence of 74-kDa bands. The data are summarized in Table 1, and an example of the SDS-PAGE analysis is presented in Fig. 1. This analysis demonstrated that the six charge–introduction substitutions Y349K, L351K, S354K, T366K, T394K, and V397K strongly interfered with homodimer formation.

Charged pairs containing these residues were constructed based on rational design (Table 2). Interacting residues were identified based on published data (9–11), and opposite charges were engineered into the complementary CH3 regions. The combinations were expressed, purified, and analyzed using native mass spectrometry (nMS). The data in Table 2 show that one pair, T366K/L351D, resulted in significant levels of bispecific antibody formation but only low levels of contaminating homodimers.

The HADDOCK docking tool and internal analysis were used to predict the contribution of additional charge interactions across a dimer interface that already contained charged substitutions at positions Thr-366 and Leu-351. HADDOCK scores for the heterodimers (AB) and homodimer combinations (AA and BB) were calculated for each variant pair as listed in Table 3. HADDOCK scores for the charged pair substitu-

Table 1

Substitutions constructed in the CH3 region of full-length IgG and interpretation of SDS-PAGE data

SDS-polyacrylamide gels were analyzed for the presence of a band at ~74 kDa, indicative of a substitution that impairs homodimer formation; see Fig. 1 for examples. Effect on homodimer formation was scored from +++ (strong) to − (absent).

Substitutions	Effect on homodimer formation
Q347K	−
Y349D	+/−
Y349K	+/−
T350K	−
T350K,S354K	+/−
L351K,S354K	+/−
L351K,T366K	++
L351K,P352K	+/−
L351K,P353K	++
S354K,Y349K	++
D356K	−
E357K	−
S364K	++
T366K,L351K	++
T366K,Y407K	+++
L368K	Nd
L368K,S364K	++
N390K,S400K	+/−
T394K,V397K	+
T394K,F405K	+++
T394K,Y407K	+++
P395K,V397K	+/−
S400K	−
F405K	+++
Y407K	++
Q347K, V397K, T394K	++
Y349D, P395K, V397K	++
T350K, T394K, V397K	Nd
L351K, S354K, S400K	++
S354K, Y349K, Y407K	++
T350K, N390K, S400K	+
L368K, F405K	++
D356K, T366K, L351K	+++
Q347K,S364K	++
L368D,Y407F	++
T366K	++
L351K, S354K, T366K	+++
Y349D,Y407D	++
Y349D, S364K, Y407D	++
Y349D, S364K, S400K, T407D	++

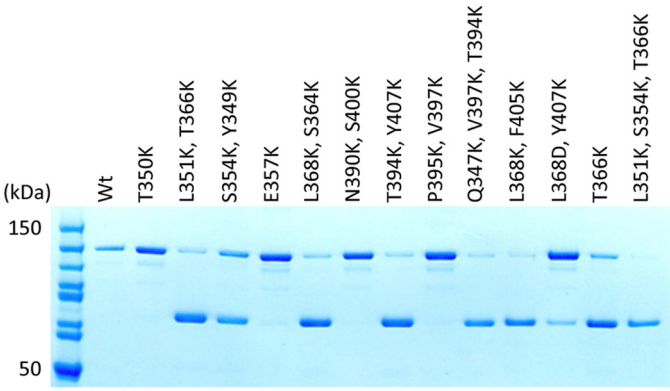

Figure 1. Identification of CH3 residues that block IgG homodimer formation. Constructs contain CH3 substitutions as indicated. Constructs containing CH3 interfaces that allow homodimer formation are visible as bands at 144 kDa, whereas interference with dimer formation is demonstrated by the presence of 74-kDa bands. *Wt* denotes wild-type IgG_1.

tions (AB) ranged from −207.5 to −255.2, and scores for the homodimers ranged from −179.5 to −228.4.

Variants that had low HADDOCK scores for the Fc heterodimeric (AB) pairs, and those that had large differences between the scores of the heterodimeric (AB) and the homodimeric pairs (AA and BB) were inserted into an expression cassette and expressed. The resulting IgG proteins were analyzed by nMS for the presence of heterodimers (AB), homodimers (AA and BB), and monomers (A and B). The data in Table 3 show that bispecific (AB) antibody levels ranged from 87 to 100%. Varying levels of homodimers and monomers, *i.e.* half-IgG molecules, were observed in these samples.

The six Fc variant pairs that had the highest levels of bispecific IgG were further characterized by subjecting them to stress conditions and analyzing the aggregation and unfolding of the bispecific IgG molecules. The variants showed very few aggregates, neither before the application of stress nor after five freeze-thaw cycles, as detected by Nile Red microscopy and 90° light scattering (Table 4). The variants were very stable when subjected to thermally induced aggregation. The antibodies were incubated for 2 days at 50 °C, an aggressive stress of which few antibodies are known to survive.[4] Indeed, following these stress conditions, we saw aggregation or unfolding of the IgG protein for most of the Fc variant pairs. However, for one variant pair (L351D,L368E/T366K,L351K), the levels of aggregation and unfolding were similar to those detected for natural human IgG_1. The β half-life of this variant pair in mice was also similar to that of native human IgG_1 (Table 4). For this variant pair, which we referred to as DEKK, the CH3 melting temperature was 69.5 °C.

DNA encoding the DEKK Fc variant pair was transfected in skewed ratios to study the effect of such skewing on hetero- and homodimer formation. When the levels of DNA encoding the two Fc variant genes were identical, the expression of the bispecific DEKK IgG species was consistently found to be 99% (Fig. 2*B*). Overexpression of one or the other Fc variants resulted in only ~70% of correctly assembled DEKK IgG in the purified IgG samples. Samples resulting from overexpression of the Fc variant containing the L351D,L368E substitutions contained up to 25% of the homodimer dubbed DEDE (Fig. 2*A*), whereas samples resulting from overexpression of the Fc variant containing the T366K,L351K substitutions also contained "KK" half-IgG molecules (Fig. 2*C*).

To obtain detailed structural information of the interactions that promote heterodimer formation, we solved the crystal structures of the DEKK Fc region and of the homodimeric Fc by-product that had mutations L351D,L368E in both chains (referred to as DEDE). To resolve the asymmetry at the dimerization interface, Fc DEKK was crystallized with the Fc-III peptide (Fig. 3) (12) bound as recently published by Leaver-Fay *et al.* (13). The crystal structure of DEKK with the Fc-III peptide bound was determined at a 2.3-Å resolution and that of

[4] Therapeomic Inc., unpublished data.

Table 2

Overview of nMS results showing relative quantification of homo- and heterodimers and half-IgG molecules for four combinations of modified heavy chains

The total amount of all bivalent IgG species (heterodimers and homodimers) was set at 100%, whereas the amount of monovalent species, or half-IgGs, was calculated as a percentage relative to the amount of bivalent IgG species. AA, AB, and BB denote dimers resulting from interactions of the A and B chains; A and B denote half-IgG.

Chain A	Chain B	AA	AB	BB	A	B
T366K	L351D	0.0	91.2	8.8	31.2	0.0
L351K	T366D	31.9	55.0	13.2	0.0	0.0
S354K,Y349K	S354D,Y349D	4.0	58.2	37.8	2.5	1.3
T394K	V397D	27.5	57.5	15.0	0.0	1.3

Table 3

HADDOCK scores and nMS data

HADDOCK scores are the weighted calculated energy values used to rank the Fc variant pairs, with higher scores indicating lower affinities between the interacting surfaces. In the nMS columns, AA, BB, and AB denote homo- and heterodimers resulting from expression of the Fc variant pairs. A and B denote half-IgGs. The total amount of all bivalent IgG species (heterodimers and homodimers) was set at 100%, and the amount of the monovalent species, or half-IgGs, was calculated as a percentage relative to the amount of bivalent IgG species.

		HADDOCK			nMS				
A	B	score AB	score AA	score BB	AA	AB	BB	A	B
WT	WT	−208.2	−208.2	−208.2					
T366K	L351D	−210.6	−191.7	−212.5	0.0	97.2	2.8	0.1	0.0
T366K	L351D,Y349D	−218.7	−191.7	−204.9					
T366K	L351D,Y349E	−215.9	−191.7	−190	1.5	97.7	0.8	4.4	0.3
T366K	L351D,L368D	−220.3	−191.7	−204.3					
T366K	L351D,L368E	−223.3	−191.7	−198.9	0.0	100.0	0.0	13.4	0.0
T366K	L351E,Y349E	−214.5	−191.7	−187.5	2.1	97.9	0.0	12.2	0.0
T366K	L351E,L368E	−214.2	−191.7	−211					
T366K	L351D,Y349E,L368E	−207.5	−191.7	−179.5	1.6	97.7	0.7	4.6	0.0
T366K	L351D,R355D	−213.3	−191.7	−211.9					
T366K	L351D,S354A,R355D	−215.5	−191.7	−209.6					
T366D	L351K,Y349K	−214.9	−198.1	−221.3					
T366D	L351K,L368K	−237.9	−198.1	−228.4	3.0	94.7	2.4	2.4	0.0
T366K,L351K	L351D	−233.2	−205.0	−212.5	0.0	86.9	13.1	11.8	0.8
T366K,L351K	L351E	−227.4	−205	−217.9					
T366K,L351K	L351D,Y349D	−255.2	−205	−204.3	1.1	98.3	0.7	3.8	0.4
T366K,L351K	L351D,Y349E	−227.2	−205	−190	0.4	98.0	1.6	3.8	0.9
T366K,L351K	L351D,L368E	−243.9	−205	−198.9	0.0	100.0	0.0	8.9	0.0
T366K,L351K	L351E,L368E	−228.9	−205	−211					
T366K,L351K	L351D,R355D	−233.6	−205	−211.9	0.0	90.7	9.3	11.4	1.6
T366K,L351K	L351D,Y349D,R355D	−242.8	−205	−183.5	1.1	97.7	1.2	3.3	0.9
T366K,L368K	L351D	−220.9	−220.7	−212.5					
T366E,L351E	L351K	−233.6	−203	−224.4					

Table 4

Biophysical analyses following accelerated stress conditions of six Fc variant pairs and wild-type human IgG_1

Combinations of the Fc variant pairs are indicated. Two days at 50 °C or five freeze-thaw (5×FT) cycles were used to stress the proteins and compare the result with protein stored at 4 °C. The formation of sub-visible aggregates was detected by Nile Red fluorescence microscopy, 90° light scatter, and 1,8-ANS fluorescence spectroscopy. Melting temperatures of CH3 regions were measured using DSC and the β half-life (β_HL in hours) was determined in mice. cps is counts/s. ND means not determined.

					1,8-ANS fluorescence				
A	B	Stress	Nile Red	90° light scatter	1,8-ANS intensity	λ maximum	Shift (nm) to 4°	CH3 T_m	β_HL
			particles/μl	*×10⁷ cps*	*×10⁶ cps*	*nm*		*°C*	*h*
WT	WT	4 °C	10–20	1.1	5.1	521	0	82.5	204/421[a]
		5 × FT	30–50	2	5.1	521			
		2 days 50 °C	10–20	0.7	5.1	521			
T366K	L351D,Y349E	4 °C	20–30	1	5.6	515		ND	ND
		5 × FT	>2000[b]	1.2					
		2 days 50 °C	>2000[b]	0.9	6.2	513	−2		
T366K	L351E,Y349E	4 °C	20–30	1	7.5	505		66.6	92
		5 × FT	>2000[b]	1.2					
		2 days 50 °C	>3000[b]	1	7.5	505	0		
T366K,L351K	L351D,Y349D	4 °C	30–50	1	7.0	505		63.4	111
		5 × FT	20–30	1.1					
		2 days 50 °C	150–200	1.1	8.7	499	−6		
T366K,L351K	L351D,Y349E	4 °C	20–30	0.9	7.6	506		64.3	128
		5 × FT	>2000[b]	1.2					
		2 days 50 °C	30–50	0.9	7.7	502	−4		
T366K,L351K	L351D,L368E	4 °C	10–20	0.8	6.2	511		69.5	390
		5 × FT	30–50	0.7					
		2 days 50 °C	10–20	0.7	6.5	508	−3		
T366K,L351K	L351D,Y349D,R355D	4 °C	30–50	1	7.5	507		ND	ND
		5 × FT	>2000[b]	1.4					
		2 days 50 °C	50–100	1	8.1	500	−7		

[a] Data were measured in two groups of 12 mice.
[b] After stress, many small particles formed.

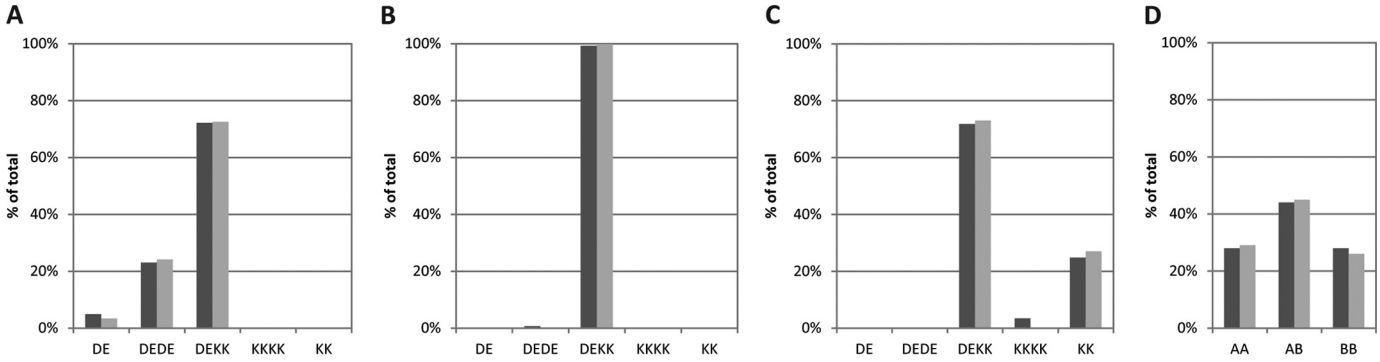

Figure 2. Efficiency of bispecific formation by DEKK. Transient transfections were performed using skewed DNA ratios of two vectors each expressing one arm of the DEKK Fc variant pair, followed by nMS analysis to determine the relative amounts of the IgG species (*A–C*). As a control, transfections were performed using two different IgG_1 heavy chains containing WT Fc regions (*D*). *Black* and *gray bars* represent duplicate experiments using different VH gene combinations in the context of the DEKK Fc variant pair or WT Fc regions. The VH gene combinations used were MF1337 × MF1122 and MF1337 × MF2729. *A,* DE/KK DNA transfection ratio 5:1; *B,* DE/KK DNA transfection ratio 1:1; *C,* DE/KK DNA transfection ratio 1:5. *DE* indicates L351D,L368E; *KK* indicates T366K,L351K. *DEDE, KKKK, DEKK, DE,* and *KK* denote the homo- and heterodimers and "half-IgGs" of the L351D,L368E and T366K,L351K arms. *D,* WT Fc regions, DNA transfection ratio 1:1. A and B denote heavy chains containing different VH regions. *AB* indicates bispecific molecules, and *AA* and *BB* indicate monospecific antibodies.

DEDE at a 2.2-Å resolution. A summary of data collection and refinement statistics is listed in Table 5. We compared these structures with a set of wild-type Fc structures (PDB codes 1L6X, 3V7M, 3AVE, 2DTS, and 1HZH (14–17)). The buried surface area of the CH3 interface in DEKK was found to be ~2,100 Å^2, which is in the same range as that of natural IgG structures, measured at 2,100 to 2,400 Å^2 (as calculated by PISA (18) using the set of wild-type Fc structures with PDB codes mentioned above). The Cα-backbone positions of DEKK differed from the Fc wild-type structures by 0.31 to 0.41 Å when the CH3 domain was superimposed separately and by 0.45 to 0.88 Å for the CH2 domain. For whole Fc fragments, the root-mean-square deviation (r.m.s.d.) increased by 0.64 to 2.50 Å, mostly due to variations in the orientation between CH3 and CH2 domains. For DEDE, the r.m.s.d. for the Cα-backbone atoms for superimposed CH3 and CH2 domains ranged from 0.25 to 0.57 Å, whereas that for the whole molecule ranged from 0.40 to 1.90 Å. The r.m.s.d. in Cα positions between DEKK and DEDE was 0.90 Å for the whole molecule, 0.22 Å for the CH3 domain, and 0.40 Å for the CH2 domain, indicating a difference in the CH3–CH2 hinge region between these two Fc crystal structures.

Fig. 3*A* shows a superimposition based on the CH3 domains of Fc DEKK and a wild-type (WT) Fc structure (PDB code 1L6X (14)). In the crystal structure of DEKK, the mutated residues L351K,T366K in chain A and L351D,L368E in chain B are clearly resolved (Fig. 3*B*). Lys-366(A) is engaged in electrostatic interactions with the mutated residues Asp-351(B) and Glu-368(B) from the opposite chain (Fig. 3*C*), as predicted by the HADDOCK model. Lys-351(A), however, is observed to interact with Pro-352(B), Ser-354(B), and Glu-357(B), in contrast to the HADDOCK-predicted interaction of Lys-351(A) with Asp-

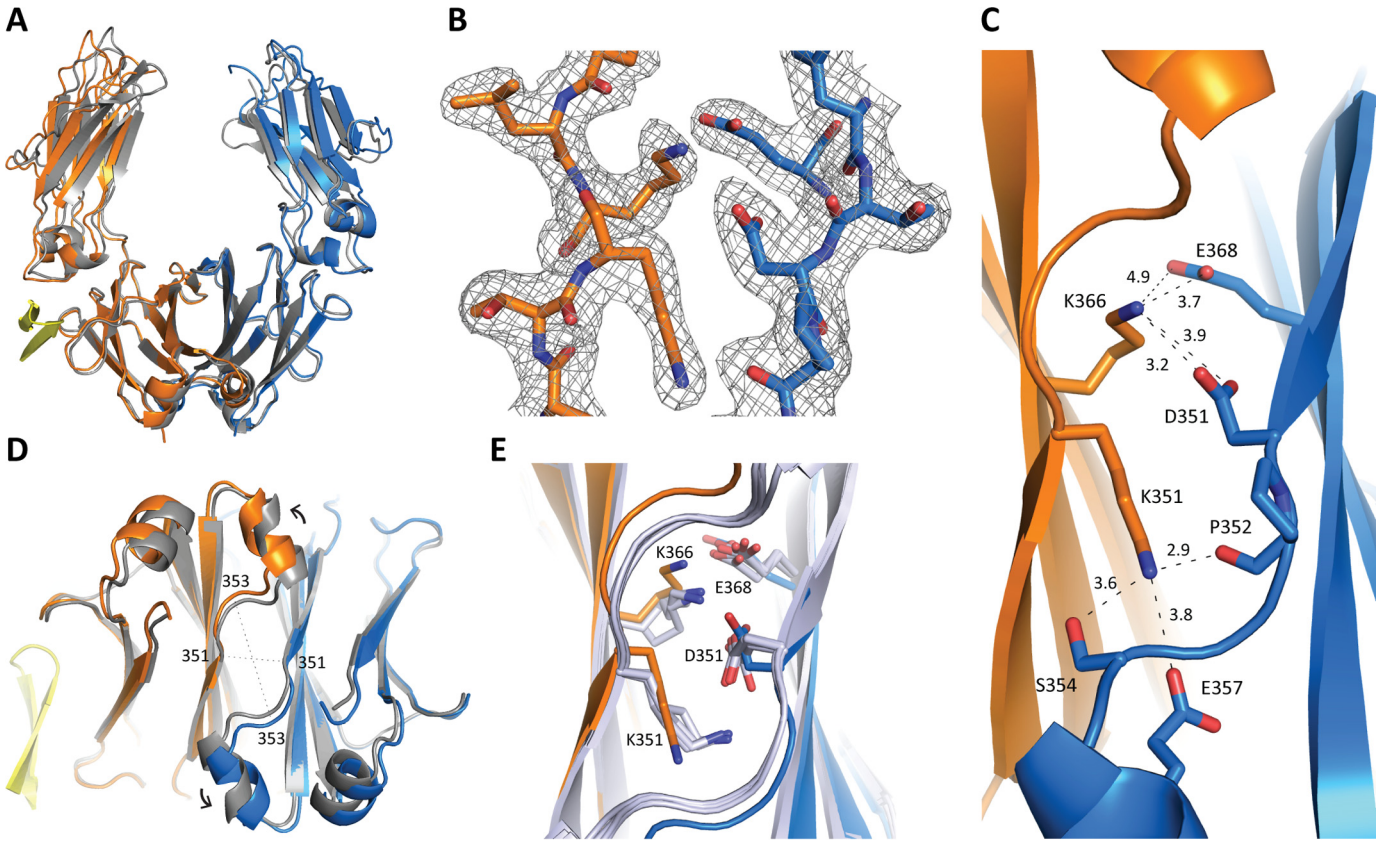

Figure 3. Crystal structure of the Fc region of DEKK at 2.3-Å resolution. *A,* structural superimposition of the DEKK and WT Fc regions (PDB code 1L6X (14)) based on CH3 domains. DEKK chain A (T366K,L351K) is colored *orange*; chain B (L351D,L368E) is *blue,* and the Fc-III peptide is *yellow*; the WT structure is *gray*. *B,* electron density ($2F_{obs} - F_{calc}$) at 1σ contour level of DEKK residues in chain A (*orange*) and in chain B (*blue*); these residues are annotated in *C*. *C,* view of the interactions within the CH3 interface of the engineered residues in DEKK (shown as *sticks*). The *dashed lines* indicate the distances between interacting atoms in Å. Color scheme as in *A*. *D,* bottom view of the CH3/CH3 dimerization interface of the superimposed structures of the DEKK and WT Fc regions (PDB code 1L6X). The *dashed lines* measure the distances between residues 351(A)-(B) and 353(A)-(B) in both DEKK and WT as provided under "Results." The *arrows* indicate the conformational rearrangement of the helix consisting of residues 354–359 in DEKK compared with the same helix in the WT molecule. Color scheme as in *A*. *E,* view of the CH3 interface of DEKK superimposed to the four best models generated by HADDOCK (*light blue*). Color scheme for DEKK as in *A*.

Table 5

Crystallographic data collection and refinement statistics

Values in parentheses are for reflections in the highest resolution shell. ASU is asymmetric unit; *CC* is correlation coefficient; r.m.s.d. is root mean square deviation. *R*free values are calculated based on 5% randomly selected reflections.

	DEKK	DEDE
Data collection		
Unit cell (Å, °)	$a = 60.1$ $b = 65.4$ $c = 78.7$ $\alpha = 90.0$ $\beta = 103.2$ $\gamma = 90.0$	$a = 50.0$ $b = 147.0$ $c = 76.4$ $\alpha = 90.0$ $\beta = 90.0$ $\gamma = 90.0$
Space group	P 1 21 1	C 2 2 21
Protein chains per ASU	2	1
Resolution (Å)	76.6–2.3 (2.4–2.3)	31.8–2.2 (2.3–2.2)
*R*merge (%)	15.4 (53.1)	5.2 (25.0)
Completeness (%)	98.7 (95.4)	99.2 (98.4)
Total no. of reflections	74,091 (7,287)	48,553 (4,163)
No. of unique reflections	26,379 (2,646)	14,188 (1,378)
Multiplicity	2.8 (2.9)	3.4 (3.3)
Mean $I/\sigma I$	3.6 (1.7)	15.9 (4.5)
*CC*1/2 (%)	97.2 (56.5)	99.8 (91.6)
Refinement		
R_{work}/R_{free} (%)	22.5/26.5	19.8/24.3
r.m.s.d. bonds (Å)	0.003	0.006
r.m.s.d. angles (°)	0.73	0.83
Mean *B*-factor (Å^2)	44.6 (27.6–77.9)	45.3 (13.0–119.9)
Ramachandran favored (%)	99.3	99.0
Ramachandran outliers (%)	0	0
Rotamer outliers (%)	0	0
Protein Data Bank code	5NSC	5NSG

351(B) (Fig. 3*E*). The Cα backbone has adjusted in the crystal structure to accommodate the mutations, yielding a modified arrangement. The central region of the interface widens in a vertical direction from 12.3 to 14 Å between Pro-353(A) and Pro-353(B), whereas across the interface region the distance between Lys-351(A) and Asp-351(B) is unchanged at 7.0 Å (Fig.

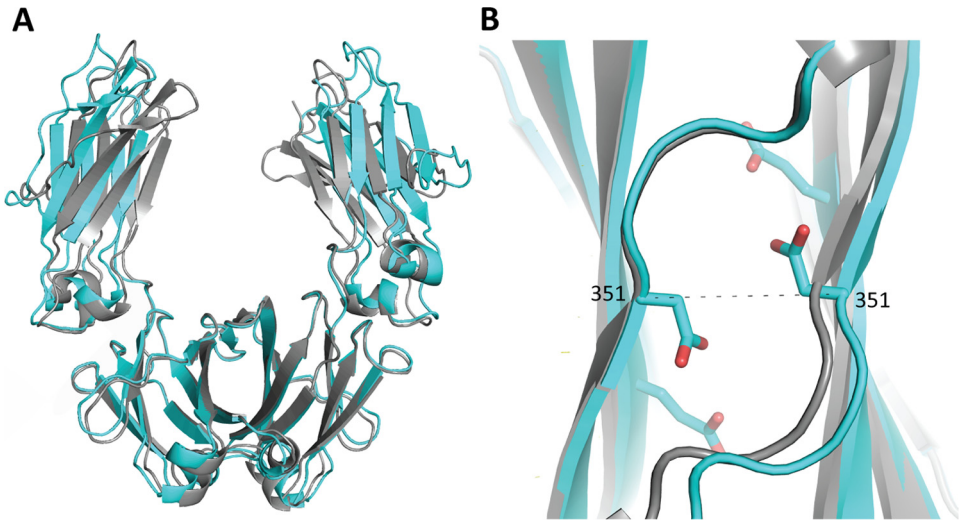

Figure 4. Crystal structure of the Fc region of DEDE at 2.2-Å resolution. *A,* structural superimposition of DEDE and WT Fc regions (PDB code 1L6X (14)), based on CH3 domains. DEDE is colored *cyan*; WT is *gray*. *B,* zoomed-in bottom view of the CH3/CH3 dimerization interface of the superimposed structures of DEDE and WT Fc regions (PDB code 1L6X), based on chain A. Mutated residues are shown as *sticks*. The *dashed lines* indicate the distance between residues 351(A)-(B) as provided under "Results."

3*D*). The changes are propagated into the helix containing residues 354–359, which shifts by ~1.5 Å, consistent with similar variations previously seen in this helix (13). It should be noted that this conformational variation does not affect the overall orientations and native interactions of the residues on the β-sheets of the CH3 interface core.

Fig. 4*A* shows the superimposition of the Fc DEDE structure and a WT Fc structure (PDB code 1L6X (14)), based on the CH3 domains. In the structure of Fc DEDE, the distance from Pro-353(A) to Pro-353(B) is 13.2 Å, which is in-between the values for DEKK and Fc WT. However, the distance from Asp-351(A) to Asp-351(B) between the β-sheets forming the core of the dimerization interface is 7.6 Å, therefore 0.6 Å larger than in DEKK and natural IgG (Fig. 4*B*).

The DEKK design was used to construct and produce a human bispecific IgG_1, named MCLA-128, at industrial scale for clinical use. Bispecific protein was expressed and purified with yields ranging from 1.0 to 1.5 g/liter and downstream processing yields ranging from 60 to 75%. A cation-exchange chromatography (CEX) step was used to remove minor residual homodimer and half-IgG contamination (Fig. 5) observed upon expression of MCLA-128 in stable CHO-DG44 BI-HEX® cells. Purity of the drug substance was high (>98.5%).

The affinities (K_D) of MCLA-128 (combining HER2 Fab MF3958 and HER3 Fab MF3178) and two control bispecific antibodies (combining, respectively, HER2 Fab MF3958 and HER3 Fab MF3178 to the tetanus toxoid Fab MF1337) were measured using Scatchard analysis. The K_D values (mean ± S.D.) from three experiments using BT-474 and SK-BR-3 cells, respectively, were 3.2 ± 0.5 and 2.0 ± 0.4 nM for MCLA-128, 3.9 ± 0.6 and 2.3 ± 0.7 nM for the HER2 × tetanus toxoid-bispecific antibody, and 0.23 ± 0.08 and 0.99 ± 0.4 nM for the HER3 × tetanus toxoid-bispecific antibody. These data show that high affinities toward HER2 and HER3 are conserved in the DEKK variant.

Accelerated stability studies were used to analyze the formulated MCLA-128 protein. The stability data indicated that DEKK-containing MCLA-128 was stable for at least 24 months at a storage temperature of 5 °C (supplemental Tables S1 and S2). Initial signs of heterogeneity only started to show up in imaged capillary isoelectric focusing after 6 months at 25 °C, and the first out-of-specification result was only observed after 12 months of exposure to 25 °C.

Discussion

The results of this study demonstrate that we could indeed design an Fc variant pair that enables efficient formation of IgG heterodimers while maintaining the stability of the native Fc region. We also show that this Fc variant pair provides an efficient platform for the generation of therapeutic bispecific antibodies in a human IgG_1 format.

In this study, experiments using charge introduction at the CH3 interface resulted in selecting residues Leu-351 and Thr-366 as candidates for further engineering; introduction of a positive charge at these positions resulted in impaired homodimerization of the IgG heavy chains. Furthermore, expression of an Fc variant pair consisting of substitutions L351D in one-half of the CH3 interface and T366K in the other resulted in bispecific IgG levels in excess of 90%. Computational analysis was used to further engineer the CH3 domains. The DEKK Fc variant pair was designed to introduce novel electrostatic interactions at the core of the heterodimeric CH3 interface such that homodimer-favoring interactions are replaced by asymmetric interactions.

The CH3 interface of the natural IgG Fc region is composed of a conserved hydrophobic core with charged residues at the rim of the interface. The crystal structure of DEKK confirms that Lys-366 in chain A is engaged in electrostatic interactions with residues Asp-351(B) and Glu-368(B) engineered in the opposite chain (Fig. 3*C*). Residue Lys-351(A) is, however, involved in interactions that were not anticipated. Instead of interacting with Asp-351(B) as predicted by the HADDOCK model, Lys-351(A) adopts a different conformation and forms electrostatic interactions with Pro-352(B), Ser-354(B), and Glu-

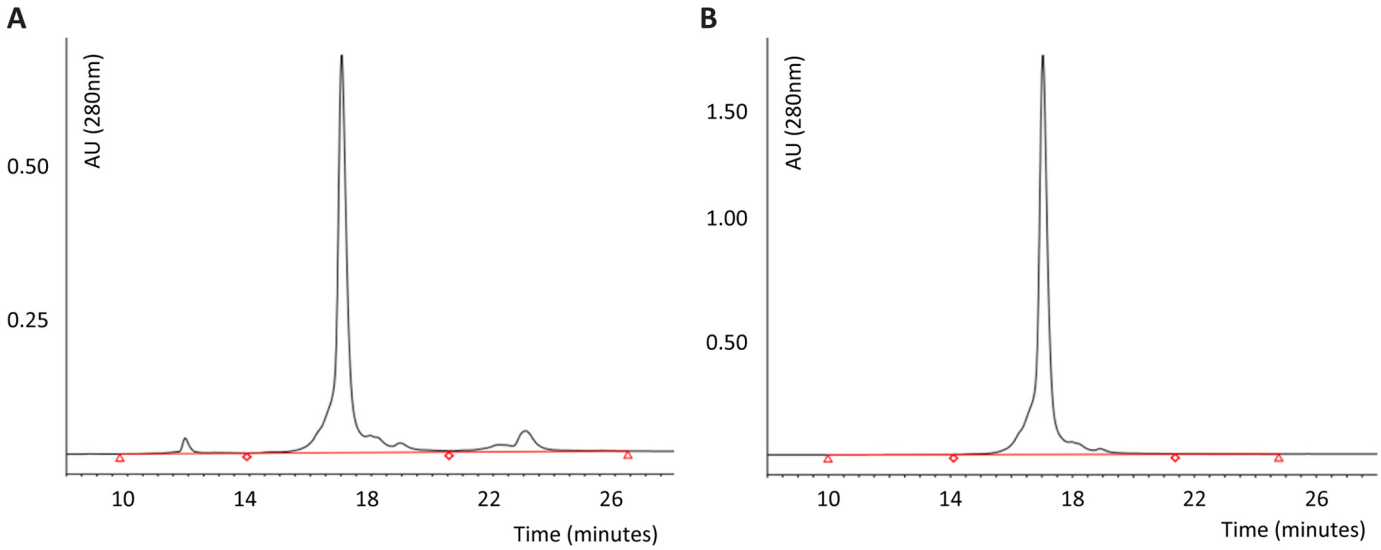

Figure 5. CEX was used to remove product-related impurities from a protein A-purified sample of MCLA-128 produced using the DEKK Fc region pair. *A,* analytical CEX chromatogram of the preparative CEX column load shows early eluting DEDE homodimers running at around 12 min, bispecific antibody MCLA-128 eluting between 14 and 20.5 min, and late eluting KK half-IgG running at around 23 min. *B,* analytical CEX chromatogram of the preparative CEX column eluate showing only bispecific antibody MCLA-128, demonstrating efficient removal of the DEDE and KK impurities. DEDE denotes the homodimer of the L351D,L368E Fc region variant, and KK denotes half-IgGs of the T366K,L351K Fc region variant.

357(B) (Fig. 3*E*). This conformation involves a rearrangement of the Cα backbone that is accommodated by a shift of the helix at residues 354–359 (Fig. 3*D*), a region of the protein also shown to have the greatest variability in previous heterodimeric Fc crystal structures (13). This movement allows the native contacts at the core of the CH3 interface to remain largely intact, which together with the novel interactions introduced in the DEKK Fc region may account for the stability of this molecule.

Structural analysis of the homodimer DEDE showed a widening in the distance between the β-sheets forming the interface core (Fig. 4*B*). This observation correlates with the charge repulsion of the four negative charges introduced in the CH3 region and is in line with the experimental observation that DEDE homodimers are only present after overexpression of the L351D,L368E heavy chains. In contrast, homodimers containing Fc region substitutions L351K,T366K in both heavy chains are virtually absent after overexpression of this variant, and the resulting proteins are primarily present as half-IgGs (Fig. 2*C*). Given the DEKK structure presented here, we hypothesize that the introduction of four lysines at the dimerization interface would cause substantial destabilization due to the long side chains causing both charge repulsion and steric hindrance. In contrast to transient productions that yield almost pure bispecific IgG (Fig. 2), the stable CHO-DG44 BI-HEX® cells expressing MCLA-128 produce both the KK and DEDE molecules in minor amounts (Fig. 5), which may result from suboptimal protein assembly in these cells (19). This figure also shows that these product-related impurities can be efficiently removed in the CEX polishing step that is routinely used in the purification of therapeutic IgG.

DEKK was selected from a panel of variants tested for optimal performance under stress conditions. When subjected to conditions that are likely to induce unfolding and precipitation (freeze-thaw cycles, incubation at 50 °C), and pharmacokinetic evaluation in mice, the behavior of the DEKK variant was found to be similar to that of natural IgG. Despite this similarity in terms of stability, the CH3 melting temperature of DEKK was only 69.5 °C, which is lower than that reported for other Fc-engineered bispecific antibodies. For example, the CH3 melting temperature of ZW1 and EW-RVT-based antibodies is ~80 °C, close to that of natural IgG. The contribution of CH3 melting temperature to the overall stability of therapeutic IgGs is therefore not clear.

We have used the DEKK substitutions to produce and purify the MCLA-128-bispecific antibody under GMP manufacturing conditions in the CHO-DG44 BI-HEX® platform (Boehringer Ingelheim), resulting in gram/liter fermentation yields. Standard IgG procedures were used to purify the protein. Purified bispecific IgG was formulated and subjected to long-term stability studies. These studies revealed the DEKK-containing MCLA-128 molecule to be highly stable. Only upon long-term exposure to 25 °C significant heterogeneity of the MCLA-128 protein could be observed, ultimately resulting in diminished binding to one of the target antigens after 12 months. However, as still only very minimal IgG fragmentation could be observed by size-exclusion chromatography at this time point (3%), this heterogeneity most likely reflects changes in the HER3 Fab domain only, and not the DEKK-containing Fc region of MCLA-128. In summary, we provide an efficient platform for the generation of therapeutic bispecific antibodies in a human IgG_1 format.

Experimental procedures

Several Fab regions were used in these studies. These Fabs were selected based on similar expression levels, proven stability, and for differences in molecular mass to facilitate the nMS analyses. All residues at the homodimerization interface within the IgG_1 CH3 region as described in Ref. 11 were designed to individually or group-wise express a lysine (positive charge) or

an aspartic acid (negative charge), see Table 1; Eu (20) numbering of residues was used throughout. A full-length cLC human IgG_1 specific for tetanus toxoid (Fab MF1337 (3)) in expression vector MV1057 (21) was used to produce the proteins. The constructs were prepared at GeneArt (Regensburg, Germany) and transiently expressed in HEK293T cells. IgGs were quantified using Fortébio Octet technology and analyzed on a non-reducing SDS-polyacrylamide gel, followed by Western blotting. Substitutions that impaired homodimer formation were identified by the presence of protein bands at ~74 kDa, corresponding to non-dimerized HC-LC complexes (half-IgG molecules).

This experiment revealed substitutions that impaired homodimer (AA) formation. We used published data (9–11) to identify residues in contact with these CH3 interface residues, and we then designed and constructed charge pairs (AB) that were introduced into vector MV1057 as described above (see also Table 2). In this experiment we also included a cLC Fab (Fab MF1025) directed against thyroglobulin. Expression was as described above, except that the expression vectors containing the designed CH3 regions and directed against tetanus toxoid and thyroglobulin were mixed in a one-to-one ratio (each individual plasmid contained a cLC expression cassette). IgGs were purified using the small-scale purification procedure described below. nMS was used to detect the presence of homo- and heterodimers (AA, BB, and AB) and half-IgG molecules (A and B), based on the mass difference of the VH regions of MF1337 (13,703 Da) and MF1025 (12,472 Da). The data (Table 2) showed that one pair (T366K/L351D) resulted in high levels of bispecific antibody formation with low levels of contaminating homodimers.

The HADDOCK docking tool (7, 8) and internal analysis were used to evaluate the effect of the proposed design changes *in silico* on the interaction between the CH3 domains of the bispecific IgG. As a structural model, we used a high-resolution crystal structure of the CH3 part of the IgG (PDB code 1L6X (14)). Design choices were introduced into this structure and evaluated using HADDOCK. The refined models were ranked according to the HADDOCK score, which is a weighted average of van der Waals energy, electrostatic energy, buried surface area, and desolvation energy. This HADDOCK score can be interpreted as an indication of affinity. HADDOCK refinement runs were performed for each designed variant pair, while assuming a rigid protein backbone and flexible amino acid residue side chains. HADDOCK scores were calculated for bispecific variant pairs (AB) as well as for homodimers (AA and BB). Preferred variants were selected based on low HADDOCK scores for the bispecific variants and high scores for the homodimer combinations (see Table 3), indicative of high and low affinities within the CH3 domain. HADDOCK-generated models were visualized using YASARA software and analyzed to gain further insight into the results and to guide design choices within the CH3 interface. The Thr-366 and Leu-351 residues were thus examined *in silico* by employing charged residues lysine, arginine, aspartic acid, and glutamic acid, and the HADDOCK scores for all resulting heterodimer and homodimer combinations were calculated. Additional design changes were analyzed at positions Tyr-349, Ser-354, Arg-355, and Leu-368, with the aim of introducing complementary charge interactions across the heterodimer interface. This resulted in a set of 11 variant pairs for which HADDOCK predicted stable heterodimer formation in the absence of homodimer contamination.

These 11 variant Fc pairs were constructed, expressed, and purified according to the medium-scale purification procedure described below. The purified samples were analyzed in nMS to establish levels of heterodimers (AB), homodimers (AA and BB), and monomers (A and B) (Table 3).

Six Fc variant pairs with optimal heterodimer/homodimer ratios were expressed and purified using the medium-scale purification procedure described below. Samples were then subjected to stress conditions and assayed as described below (listed in Table 4). Differential scanning calorimetry (DSC) was used to measure the melting temperatures of the CH3 regions (full-length IgG and Fc-hinge proteins), and a pharmacokinetics evaluation in mice was used to estimate overall stability of the molecules. The results of these assays identified the Fc variant pair DEKK as the most promising platform for production of bispecific IgG.

To study the efficiency of heterodimer formation by the Fc variant pair DEKK, transient transfections were performed using skewed DNA ratios of the two vectors expressing each arm of the Fc variant pair (5:1 to 1:5). This was followed by purification using the medium-scale procedure described below and nMS analysis to determine the relative amounts of the IgG species. This experiment was performed in duplicate using different combinations of VH genes in the context of the DEKK Fc variant pair (Fig. 2). The different VH gene combinations used were MF1337 × MF1122 and MF1337 × MF2729 specific for tetanus toxoid, fibrinogen, and RSV-F protein, respectively.

IgG expression constructs

Full-length cLC IgG_1 was prepared using MV1057-based expression vectors (21) modified with the design choices as described. Proteins containing only the IgG_1 hinge and Fc regions were used for crystallography and DSC experiments. These Fc-hinge proteins were produced using a truncated variant of MV1057 that has amino acid Glu-216 as the first residue.

Protein production

Proteins were produced in HEK293T cells using FuGENE HD transfection reagent according to the manufacturer's protocols or in Freestyle™ 293-F cells (Invitrogen) using polyethyleneimine (PEI) with a PEI/DNA mass ratio of 2.5:1. Bispecific IgGs were transfected using a 1:1 DNA mass ratio unless stated otherwise.

IgG purification

Cell supernatants were purified at different scales. Small-scale protein A purification of IgG was performed using PhyNexus tips according to the manufacturer's protocols, followed by neutralization of the acidic elution fraction using Tris. Medium-scale purification was performed using an ÄKTA Explorer 100 (GE Healthcare) equipped with HiTrap MabSelect SuRe columns and HiTrap desalting columns. After acidic

elution from the MabSelect SuRe columns, the proteins were directly desalted to PBS, pH 7.4. Purification of Fc-hinge proteins for crystallography studies was carried out using batch-wise incubation with MabSelect SuRe LX medium, followed by neutralization using Tris. In the next step, the proteins were gel-filtrated using a Superdex75 16/600 column (GE Healthcare) and concentrated using Vivaspin columns (Sartorius).

IgG quantification

IgGs (small-scale productions) were quantified using Fortébio Octet technology using protein A sensors, and human IgG (Sigma) was used for a standard curve. Medium- and large-scale produced IgGs were quantified by OD280 absorption.

SDS-PAGE/PageBlue staining

1–2 μg of protein was loaded onto a NuPAGE 4–12% Bistris gel (Invitrogen) in the presence or absence of reducing agent (Invitrogen). A protein marker was included on each gel. After running at 100–200 V, the gel was stained using PageBlue protein staining solution (Fermentas) and subsequently destained using milliQ water.

SDS-PAGE/Western blotting

0.1–1 μg of protein was loaded on a NuPAGE 4–12% Bistris gel (Invitrogen) in the presence or absence of reducing agent (Invitrogen). A pre-stained protein marker was included on each gel. After running at 100–200 V, the gel was transferred to nitrocellulose and visualized using peroxidase-labeled anti-human Fc antibody followed by enhanced chemiluminescence (ECL) detection.

DSC

DSC was used to measure the thermostability of the domains of the IgG described here. DSC experiments were performed on a MicroCal VP-DSC using Origin version 7.0 (VPViewer and VPAnalyzer) software. The purified antibodies or Fc-hinge fragments were first dialyzed against a 10 mM phosphate, 150 mM NaCl buffer, pH 6.5. The samples were analyzed at a protein concentration of 0.25 mg/ml as determined by UV absorption. Scans ran from 50 to 95 °C with a scan rate of 1 °C/min and were analyzed using GraphPad Prism 5 and Microsoft Excel 2010 software.

nMS

For nMS, the IgGs were deglycosylated to create a single product with a distinct mass suitable for mass spectrometric analysis. 1 unit of *N*-glycosidase F (Roche Diagnostics, Mannheim, Germany) was incubated per 10 μg of IgG_1, overnight at 37 °C in 0.1 M citrate buffer, pH 3.0, 1.0 M Tris-HCl, pH 8.0. Buffer exchange using 10-kDa MWCO centrifugal filter columns (Millipore) was performed to remove glycan chains and change the buffer to 150 mM ammonium acetate, pH 7.5. 3 μl of a 1 μM concentration of IgG were loaded into gold-plated borosilicate capillaries made in-house (using a Sutter P-97 puller (Sutter Instruments Co., Novato, CA) and an Edwards Scancoat six sputter-coater (Edwards Laboratories, Milpitas, CA)) for analysis on an LCT 1 mass spectrometer (Waters Corp., Milford, MA), adjusted for optimal performance in high mass detection (33). A capillary voltage of 1300 V was used, and a sampling cone voltage was 200 V. The source backing pressure was elevated to promote collisional cooling to ~7.5 mbars. Processing of the acquired spectra was performed using MassLynx 4.1 software (Waters Corp., Milford, MA). Minimal smoothing was used, after which the spectra were centered. The mass of the species was calculated using each charge state in a series. The corresponding intensities of each charge state were assigned by MassLynx and summed. All analyses were repeated three times to calculate means. This approach allowed the relative quantification of all species in a sample. Note that the total amount of bivalent IgG species was set at 100% to allow a direct comparison between these molecules, whereas the amounts of the monovalent species, or half-IgGs, were calculated as a percentage relative to the bivalent molecules.

Fluorescence microscopy with Nile Red staining

Nile Red is an uncharged small (18.37 Da) molecular mass hydrophobic fluorescence probe that allows detection of very low levels of protein aggregates (22). The IgG samples were diluted to 0.2 mg/ml and filtered using 0.22-μm PVDF sterile filters before applying the stress conditions. 0.2 μl of 100 μM Nile Red in ethanol was added to 10 μl of the IgG samples just prior to measurements. The samples were introduced in a FastRead 102™ slide (Immune Systems, UK) and analyzed by counting particles in fluorescence microscopy using a Leica DM RXE microscope (Leica Microsystems GmbH, Wetzlar, Germany) equipped with a mercury lamp and a bandpass filter cube Leica N2.1 513 812 with an excitation filter BP515-560 nm (green light) and suppression filter LP 590 nm for specific excitation of Nile Red. The FastRead 102 slides display a square grid with a mesh size of 250 μm. Particles were counted in 16 squares, which correspond to 1 × 1 mm and 0.1-μl volume. The total number of particles was multiplied by 10 to obtain the number of particles/μl.

90° light-scatter spectroscopy

The 90° light-scattering spectra of IgG solutions are known to be very sensitive to small amounts of antibody aggregates in solutions (23). The 90° light-scattering spectra of IgG solutions were measured using a FluoroMax-1 spectrofluorometer (Horiba Scientific, UK) between 400 and 750 nm with excitation and emission monochromators moving synchronously. The IgG samples were diluted to 0.2 mg/ml and filtered using 0.22-μm PVDF sterile filters before applying the stress conditions. 150 μl of sample were added to a 1-cm × 2-mm black cuvette (Hellma 105-250-QS). The aggregation state of the IgG in the samples was determined by monitoring light scattering at 400 nm after subtraction of the background. The light-scattering intensity was expressed as counts/s.

1,8-ANS fluorescence spectroscopy

1-Anilinonaphthalene-8-sulfonic acid (1,8-ANS) is an uncharged small (299.34 Da) hydrophobic fluorescent probe that is a sensitive indicator of protein folding and conformational changes, as well an indicator of antibody aggregation (24). The IgG samples were diluted to 0.2 mg/ml and filtered using 0.22-μm PVDF sterile filters before applying the stress condi-

tions. 150 μl of sample were added to a 1-cm × 2-mm black cuvette (Hellma 105–250-QS); and 3.0 μl of 2.5 mM 1,8-ANS in water were added on top (final concentration, 50 μM 1,8-ANS). The sample was measured immediately after addition of 1,8-ANS. 1,8-ANS fluorescence emission was measured after excitation at 370 nm on a FluoroMax-1 spectrofluorometer (Horiba Scientific, UK). The changes in 1,8-ANS fluorescence intensity and emission wavelength due to stress were determined.

Crystallography of Fc DEKK and DEDE variants

Prior to crystallization, the Fc-hinge construct of the DE Fc variant was modified to optimize asymmetric assembly of the DEKK Fc region into the crystal lattice. As described previously by Leaver-Fay *et al.* (13), this construct was mutated at positions M252E, I253A, and H435A to prevent binding of the DE chain to the Fc-III peptide (12) (DCAWHLGELVWCT, disulfide-oxidized, ProteoGenix). The mutated DE construct and the Fc-hinge construct expressing the KK Fc region were expressed in 293FF cells in a one-to-one ratio and purified according to the large-scale purification procedure described above. Purified Fc DEKK in 25 mM Tris, pH 7.5, and 150 mM NaCl at a concentration of 12.3 mg/ml was mixed with 1 mM Fc-III peptide (13) dissolved in the same buffer. Protein of the DEDE homodimeric Fc variant was prepared by transfecting the Fc-hinge construct containing the DE design into 293FF cells followed by purification according to the large-scale purification procedure described above. The resulting protein was concentrated to 10 mg/ml in 25 mM Tris, pH 7.5, and 150 mM NaCl. For initial crystallization trials, the protein solutions were screened using the vapor diffusion method in 96-well format plates (Corning) using commercially available screens: JCSG core suite (Qiagen), PEG/ion (Hampton Research), and Wizard (Emerald BioSystems). The initial setup combined 0.15 μl of protein with 0.15 μl of mother liquor solution using a Phoenix robot (Art Robins Instrument). Crystals appeared after 2–3 days in many conditions. Optimization screens were prepared in hanging-drop plates by varying concentrations of precipitant solutions and protein/mother liquor ratios at 18 and 4 °C. The best crystals for DEKK/Fc-III peptide were grown in 0.2 M sodium fluoride and 20% w/v PEG 3350, whereas the best crystals for DEDE were grown in acetate buffer, pH 4.5, 0.2 M zinc acetate, and 16% w/v PEG 3000. A protein/precipitant ratio of 1:1 and a temperature of 18 °C were used in both cases. Crystals were transferred to a cryo-protectant solution containing mother liquor and 20% v/v glycerol prior to shock-cooling in liquid nitrogen. Diffraction data were collected at the European Synchrotron Research Facility (ESRF) at ID29 beamline for DEKK and at ID23-2 beamline for DEDE. Diffraction data were processed using IMOSLFM (25) and AIMLESS (26) software. Structures were solved by molecular replacement in PHASER MR (27) software, using the published heterodimeric Fc complex with the Fc-III peptide (PDB code 5DK0 (13)) as a search model for DEKK, and an Fc wild-type structure (PDB code 4CDH (28)) for DEDE. The resulting solutions were refined using PHENIX (29) software, and model building was carried out using COOT (30) software. The structure figures were generated using PyMOL (31).

Pharmacokinetics

Pharmacokinetic characteristics of the bispecific IgGs were analyzed in non-target antigen-bearing female BALB/c mice of ~7 weeks of age after a single intravenous injection. Groups of 12 mice were dosed at 1 mg/kg; each group consisted of three subgroups of four mice and from each mouse six time points were sampled. Blood samples were collected pre-dose and 0.25, 1, 2, 4, 8, 24, 48, 96, 168, 268, and 336 h after dosing. IgG levels in sera were established by ELISA (ZeptoMetrics, New York). Data were analyzed using SpectraMax software to establish C_{max} (μg/ml) and α- and β-half-life (h).

Large-scale fermentation and purification

MCLA-128 was produced at Boehringer Ingelheim Biopharmaceuticals (Biberach a.d. Riss, Germany) using their BI-HEX® mammalian IgG expression platform. MCLA-128 was expressed in Chinese hamster ovary (CHO) DG44 cells stably co-expressing the cLC, the different heavy chains, and the RMD enzyme (GDP-6-deoxy-D-lyxo-4-hexulose reductase), thereby yielding antibodies with a low level of fucose on their CH2 region-associated glycan structures. MCLA-128 drug substance was produced in a 2,000-liter stainless steel bioreactor using a 14-day fed-batch process. The MCLA-128 protein was purified using a standard IgG manufacturing process involving protein A capture chromatography, a low-pH hold step for virus inactivation, anion-exchange chromatography in flow-through mode, and CEX. This last chromatography step was used to remove minor residual homodimer and half-IgG contamination. After a 20-nm virus filtration step, MCLA-128 was concentrated and formulated at 20 mg/ml following ultrafiltration/diafiltration and addition of the final excipients. MCLA-128 drug product was filled in 6R type I glass vials at 20 mg/ml at a nominal fill volume of 5 ml.

Affinities

Scatchard analyses were performed to establish the affinities (K_D) of MCLA-128 (combining HER2 Fab MF3958 and HER3 Fab MF3178) and two control bispecific antibodies (combining, respectively, HER2 Fab MF3958 and HER3 Fab MF3178 to the tetanus toxoid Fab MF1337) (32). Briefly, the antibodies were radiolabeled with ^{125}I using IODO-GEN® precoated iodination tubes (Pierce) according to the manufacturer's instructions. Flow cytometry using BT-474 and SK-BR-3 cells, which express both HER2 and HER3, was used to confirm that the binding activity of the radiolabeled antibodies was conserved compared with the non-labeled molecules. Affinities were measured by seeding SK-BR-3 or BT-474 cells in 96-well plates. The next day, the cells were incubated with a titration range of the antibodies for 4 h at 4 °C. Unbound radioactivity was removed, and cell-bound radioactivity was measured using a gamma well counter. Non-specific binding was measured by adding a 100-fold excess of unlabeled antibody. Each condition was tested in triplicate, and three independent experiments were performed per antibody. K_D values were calculated based on a non-linear regression model that compensates for non-specific binding (Prism 6.0, GraphPad).

Stability

To determine the shelf life of the MCLA-128 drug product, stability studies were performed according to the International Conference on Harmonization guidelines. Stability was analyzed at the proposed long-term storage temperature (5 ± 3 °C) and under accelerated conditions (25 ± 2 °C). The analytical procedures used are listed in supplemental Tables S1 and S2.

Author contributions—C. D. N. performed the crystallography experiments. L. J. A. H. performed cloning, HADDOCK modeling, and biophysical assays. E. P. conducted the stability assays. All three contributed to writing the paper. T. A., P. G., A. B. H. B., and J. d. K. were responsible for design of experiments, interpretation of results, and writing of the paper.

Acknowledgments—We are grateful to the European Synchrotron Radiation Facility (ESRF) for the provision of synchrotron radiation facilities and to beamline scientists at the ESRF and the European Molecular Biology Laboratory for assistance. We thank Tim de Klijn for the useful discussions.

References

1. Beck, A., Wurch, T., Bailly, C., and Corvaia, N. (2010) Strategies and challenges for the next generation of therapeutic antibodies. *Nat. Rev. Immunol.* **10,** 345–352
2. Kontermann, R. (2012) Dual targeting strategies with bispecific antibodies. *MAbs* **4,** 182–197
3. de Kruif, J., Kramer, A., Visser, T., Clements, C., Nijhuis, R., Cox, F., van der Zande, V., Smit, R., Pinto, D., Throsby, M., and Logtenberg, T. (2009) Human immunoglobulin repertoires against tetanus toxoid contain a large and diverse fraction of high-affinity promiscuous VH genes. *J. Mol. Biol.* **387,** 548–558
4. Ha, J.-H., Kim, J.-E., and Kim, Y.-S. (2016) Immunoglobulin Fc heterodimer platform technology: from design to applications in therapeutic antibodies and proteins. *Front. Immunol.* **7,** 394
5. Spiess, C., Merchant, M., Huang, A., Zheng, Z., Yang, N.-Y., Peng, J., Ellerman, D., Shatz, W., Reilly, D., Yansura, D. G., and Scheer, J. M. (2013) Bispecific antibodies with natural architecture produced by co-culture of bacteria expressing two distinct half-antibodies. *Nat. Biotechnol.* **31,** 753–758
6. Smith, E. J., Olson, K., Haber, L. J., Varghese, B., Duramad, P., Tustian, A. D., Oyejide, A., Kirshner, J. R., Canova, L., Menon, J., Principio, J., MacDonald, D., Kantrowitz, J., Papadopoulos, N., Stahl, N., *et al.* (2015) A novel, native-format bispecific antibody triggering T-cell killing of B-cells is robustly active in mouse tumor models and cynomolgus monkeys. *Sci. Rep.* **5,** 17943
7. Dominguez, C., Boelens, R., Bonvin, A. M. (2003) HADDOCK: a protein-protein docking approach based on biochemical or biophysical information. *J. Am. Chem. Soc.* **125,** 1731–1737
8. van Zundert, G. C., Rodrigues, J. P., Trellet, M., Schmitz, C., Kastritis, P. L., Karaca, E., Melquiond, A. S., van Dijk, M., de Vries, S. J., Bonvin, A. M. (2016) The HADDOCK2.2 web server: user-friendly integrative modeling of biomolecular complexes. *J. Mol. Biol.* **428,** 720–725
9. Miller, S. (1990) Protein-protein recognition and the association of immunoglobulin constant domains. *J. Mol. Biol.* **216,** 965–973
10. Deisenhofer, J. (1981) Crystallographic refinement and atomic models of a human Fc fragment and its complex with fragment B of protein A from *Staphylococcus aureus* at 2.9- and 2.8-Å resolution. *Biochemistry* **20,** 2361–2370
11. Gunasekaran, K., Pentony, M., Shen, M., Garrett, L., Forte, C., Woodward, A., Ng, S. B., Born, T., Retter, M., Manchulenko, K., Sweet, H., Foltz, I. N., Wittekind, M., and Yan, W. (2010) Enhancing antibody Fc heterodimer formation through electrostatic steering effects applications to bispecific molecules and monovalent IgG. *J. Biol. Chem.* **285,** 19637–19646
12. DeLano, W. L., Ultsch, M. H., de Vos, A. M., and Wells, J. A. (2000) Convergent solutions to binding at a protein-protein interface. *Science* **287,** 1279–1283
13. Leaver-Fay, A., Froning, K. J., Atwell, S., Aldaz, H., Pustilnik, A., Lu, F., Huang, F., Yuan, R., Hassanali, S., Chamberlain, A. K., Fitchett, J. R., Demarest, S. J., and Kuhlman, B. (2016) Computationally designed bispecific antibodies using negative state repertoires. *Structure* **24,** 641–651
14. Idusogie, E. E., Presta, L. G., Gazzano-Santoro, H., Totpal, K., Wong, P. Y., Ultsch, M., Meng, Y. G., and Mulkerrin, M. G. (2000) Mapping of the C1q binding site on rituxan, a chimeric antibody with a human IgG1 Fc. *J. Immunol.* **164,** 4178–4184
15. Sibéril, S., Ménez, R., Jorieux, S., de Romeuf, C., Bourel, D., Fridman, W. H., Ducancel, F., Stura, E. A., and Teillaud, J. L. (2012) Effect of zinc on human IgG1 and its FcγR interactions. *Immunol. Lett.* **143,** 60–69
16. Matsumiya, S., Yamaguchi, Y., Saito, J., Nagano, M., Sasakawa, H., Otaki, S., Satoh, M., Shitara, K., and Kato, K. (2007) Structural comparison of fucosylated and nonfucosylated Fc fragments of human immunoglobulin G1. *J. Mol. Biol.* **368,** 767–779
17. Saphire, E. O., Parren, P. W., Pantophlet, R., Zwick, M. B., Morris, G. M., Rudd, P. M., Dwek, R. A., Stanfield, R. L., Burton, D. R., and Wilson, I. A. (2001) Crystal structure of a neutralizing human IGG against HIV-1: a template for vaccine design. *Science* **293,** 1155–1159
18. Krissinel, E., and Henrick, K. (2007) Inference of macromolecular assemblies from crystalline state. *J. Mol. Biol.* **372,** 774–797
19. Mason, M., Sweeney, B., Cain, K., Stephens, P., and Sharfstein, S. T. (2012) Identifying bottlenecks in transient and stable production of recombinant monoclonal-antibody sequence variants in Chinese hamster ovary cells. *Biotechnol. Prog.* **28,** 846–855
20. Kabat, E. A., Wu, T. T., Perry, H. M., Gottesman, K. S., and Foeller, C. (1991) *Sequences of Proteins of Immunological Interest*. United States Public Health Service, 5th Ed., National Institutes of Health, Bethesda
21. de Kruif, J., Kramer, A., Nijhuis, R., van der Zande, V., den Blanken, R., Clements, C., Visser, T., Keehnen, R., den Hartog, M., Throsby, M., and Logtenberg, T. (2010) Generation of stable cell clones expressing mixtures of human antibodies. *Biotechnol. Bioeng.* **106,** 741–750
22. Demeule, B., Gurny, R., and Arvinte, T. (2007) Detection and characterization of protein aggregates by fluorescence microscopy. *Int. J. Pharm.* **329,** 37–45
23. Demeule, B., Lawrence, M. J., Drake, A. F., Gurny, R., and Arvinte, T. (2007) Characterization of protein aggregation: the case of a therapeutic immunoglobulin. *Biochim. Biophys. Acta* **1774,** 146–153
24. Demeule, B., Palais, C., Machaidze, G., Gurny, R., and Arvinte, T. (2009) New methods allowing the detection of protein aggregates. *MAbs* **1,** 142–150
25. Battye, T. G. G., Kontogiannis, L., Johnson, O., Powell, H. R., and Leslie, A. G. W. (2011) iMOSFLM: a new graphical interface for diffraction-image processing with MOSFLM. **67,** 271–281
26. Evans, P. R. (2011) An introduction to data reduction: space-group determination, scaling and intensity statistics. *Acta Crystallogr. D Biol. Crystallogr.* **67,** 282–292
27. McCoy, A. J., Grosse-Kunstleve, R. W., Adams, P. D., Winn, M. D., Storoni, L. C., and Read, R. J. (2007) Phaser crystallographic software. *J. Appl. Crystallogr.* **40,** 658–674
28. Silva-Martín, N., Bartual, S. G., Ramírez-Aportela, E., Chacón, P., Park, C. G., and Hermoso, J. A. (2014) Structural basis for selective recognition of endogenous and microbial polysaccharides by macrophage receptor SIGN-R1. *Structure* **22,** 1595–1606
29. Adams, P. D., Afonine, P. V., Bunkóczi, G., Chen, V. B., Davis, I. W., Echols, N., Headd, J. J., Hung, L.-W., Kapral, G. J., Grosse-Kunstleve, R. W., McCoy, A. J., Moriarty, N. W., Oeffner, R., Read, R. J., Richardson, D. C., Richardson, J. S., Terwilliger, T. C., and Zwart, P. H. (2010) PHENIX: A comprehensive Python-based system for macromolecular structure solution. *Acta Crystallogr. D Biol. Crystallogr.* **66,** 213–221

30. Emsley, P., Lohkamp, B., Scott, W. G., and Cowtan, K. (2010) Features and development of Coot. *Acta Crystallogr. D Biol. Crystallogr.* **66,** 486–501
31. Schrödinger, LLC (2012) The PyMOL Molecular Graphics System, Version 1.5.0, Schrödinger, LLC, New York
32. Heskamp, S., van Laarhoven, H. W., Molkenboer-Kuenen, J. D., Bouwman, W. H., van der Graaf, W. T., Oyen, W. J., and Boerman, O. C. (2012) Optimization of IGF-1R SPECT/CT imaging using ^{111}In-labeled F(ab′)$_2$ and Fab fragments of the monoclonal antibody R1507. *Mol. Pharm.* **9,** 2314–2321
33. Tahallah, N., Pinkse, M., Maier, C. S., and Heck, A. J. R. (2001) The effect of the source pressure on the abundance of ions of noncovalent protein assemblies in an electrospray ionization orthogonal time-of-flight instrument. *Rapid Commun. Mass Spectrom.* **15,** 596–601

A new approach for generating bispecific antibodies based on a common light chain format and the stable architecture of human immunoglobulin G 1

Camilla De Nardis, Linda J. A. Hendriks, Emilie Poirier, Tudor Arvinte, Piet Gros, Alexander B. H. Bakker and John de Kruif

J. Biol. Chem. 2017, 292:14706-14717.
doi: 10.1074/jbc.M117.793497 originally published online June 27, 2017